

RESEARCH ARTICLE

Improving the Modified XFEM for Optimal High-Order Approximation

Ben A. Saxby* | Andrew L. Hazel

Department of Mathematics, The University of Manchester, Manchester, UK

Correspondence

*Ben Saxby, Cubic Motion, Room 117/118
N/P Block, Pinewood Studios, Pinewood
Road, Iver Heath, SL0 0NH.
Email: ben.saxby@alumni.manchester.ac.uk

Abstract

This paper investigates the accuracy of high-order extended finite element methods (XFEMs) for the solution of discontinuous problems with both straight and curved weak discontinuities in two dimensions. The modified XFEM is found to offer advantages in cost and complexity over other approaches, but suffers from suboptimal rates of convergence due to spurious higher order contributions to the approximation space. An improved modified XFEM is presented, with basis functions ‘corrected’ by projecting out higher order contributions that cannot be represented by the standard finite element basis. The resulting corrections are independent of the equations being solved. An accurate numerical integration scheme that correctly integrates functions with curved discontinuities is also presented. Optimal rates of convergence are then recovered for Poisson problems with both straight and quadratically curved interfaces for approximations up to order $p \leq 4$. These are the first truly optimal convergence results achieved using the XFEM for a curved weak discontinuity, and also the first optimally convergent results achieved using the modified XFEM for any problem with approximations of order $p > 1$. Almost optimal rates of convergence are recovered for an elastic problem with a circular weak discontinuity for approximations up to order $p \leq 4$.

KEYWORDS:

extended finite element method; high-order accuracy; curved weak discontinuity; optimal convergence

1 | INTRODUCTION

High-order methods for the solution of partial differential equations offer huge potential for increased accuracy^{1,2}. Provided the problem is sufficiently smooth, a higher order finite/spectral element method can approximate the solution to a much higher degree of accuracy than a low order method for comparable cost³. A p -order accurate method is defined as one in which the error in the approximate solution reduces with the mesh spacing h at a rate $O(h^p)$ in the H^1 norm. The definition of a high-order method is generally regarded as being one that is third-order or higher¹.

Optimal rates of convergence for higher order approximations to smooth problems are straightforward to obtain⁴. Our aim is to achieve the same optimal rates of convergence for higher order approximations to problems with arbitrarily aligned discontinuities. Such problems arise in several areas, including crack propagation^{5,6} and multi-phase fluid flow problems⁷. The standard finite element method (FEM) is unable to accurately resolve kinks or jumps in the solution in element interiors⁴. Instead we

can either align the FE mesh with the discontinuity, or enrich the FE approximation space in order to accurately represent the discontinuity independent of the mesh.

The use of a mesh with element boundaries aligned with the discontinuity allows kinks in the solution to be handled naturally by the finite element method because it permits jumps in gradient of the solution across element boundaries. However, if a time-dependent problem is to be solved, particularly one in which the location of the discontinuity changes with time, then the mesh must be updated continually in response to the movement of the interface. We call this an interface-tracking method. In contrast, with the enriched approach the mesh need not change as the interface moves. However, simply using the standard finite element basis functions on an unfitted mesh results in an approximation space that is unable to accurately represent the discontinuous solution, as is demonstrated later in section 4. Instead, the enriched basis functions must be updated to incorporate the moving discontinuity. We call this an interface-capturing method because the interface is immersed in the fixed background mesh and its location is ‘captured’ implicitly.

The application of boundary-fitted methods suffers from the need to solve the equations governing the motion of the mesh in response to the prescribed boundary deformation together with those of the physical problem, which can be costly. Furthermore, if the interface undergoes large deformations then remeshing is required and this can be problematic⁸. If instead an immersed method is used, then none of the costly update or remeshing procedures associated with boundary-fitted methods are required. However, an additional auxiliary function is required that is defined over the whole domain. Storing and updating this function increases the memory requirements and cost of the method. The size of the approximation space for immersed methods is also larger than that for boundary-fitted methods, thus also increasing the problem size.

In this paper we focus on the use of immersed methods to model discontinuities independently of the mesh. We use the level set method^{9,10} to capture the location of the discontinuity and the extended finite element method (XFEM)^{5,11} to incorporate the discontinuity into the finite element approximation space.

Note that, although immersed methods can be used for steady problems (e.g. to simplify the meshing of complex geometries^{12,13}), typically boundary-fitted methods are preferred. Our use of immersed methods here is motivated instead by the potential for their extension to time-dependent problems for which they are better-suited. In this paper we use the XFEM to solve some simple steady discontinuous problems with the aim of achieving the same optimal rates of convergence as can be achieved using the standard FEM for smooth problems. That is, we expect to achieve rates of convergence of order $O(h^p)$, where h is the mesh spacing and p is the polynomial order of the approximation.

In section 2 we introduce the XFEM approximation and some possible enrichment functions. We also discuss the current state of knowledge according to the literature. Next, in section 3, we introduce a Poisson problem with a discontinuity that is used throughout this paper to evaluate the performance of our XFEM with respect to an analytic solution. Then in section 4 we compare the performance of some XFEMs in two dimensions and demonstrate how the modified XFEM converges suboptimally. We also present an improvement to the modified XFEM that recovers optimal rates of convergence for the Poisson problem with a straight discontinuity. In section 5 we consider a Poisson problem with a quadratically curved discontinuity and generalise both the integration scheme and our corrections to the modified XFEM for curved discontinuities. We then present optimally convergent results. The resulting corrections are independent of the equations to be solved, in contrast to assumed strain projection methods^{7,14}. In section 6 we consider a two-dimensional linear elasticity problem with a circular discontinuity which recovers almost optimally convergent results. Finally, our conclusions are presented in section 7.

2 | XFEM APPROXIMATION

The extended finite element method is based on the partition of unity (PU) concept proposed by Babuška et al.^{15,16}. It uses a priori information about the form and location of the discontinuity to incorporate additional functions into the standard finite element approximation space. The XFEM approximation takes the form

$$u^h(x) = \sum_i u_i \psi_i(x) + \sum_i u_i^* \Psi(x) N_i(x), \quad (1)$$

where $u_i \in \mathbb{R}$ are the standard FE unknowns, ψ_i are the standard FE basis functions, $u_i^* \in \mathbb{R}$ are the enriched unknowns, Ψ is a global enrichment function that represents the discontinuity that is to be included, and $\{N_i\}$ forms a PU over the domain. That is, $\sum_i N_i(x) \equiv 1$. This PU property allows the global enrichment function Ψ to be reproduced exactly in the XFEM approximation. Often N_i are chosen to be equal to ψ_i . This ensures that they form a global partition of unity over Ω , although the resulting

method is not as general as the PUM/PUFEM^{17,18}. We call the functions $\psi_i^* = \Psi\psi_i$ the local enrichment functions because their support is restricted to that of the standard FE basis functions.

Let us describe the location Γ of the discontinuity by the zero level set of a function ϕ defined over the whole domain Ω . That is, $\Gamma = \{\mathbf{x} \in \Omega \mid \phi(\mathbf{x}) = 0\}$. We can then use this level set function ϕ to characterise the discontinuity. Note that in practice we use the discretised level set function $\phi^h = \sum_i \phi_i \psi_i$ rather than ϕ itself. The Kronecker- δ property of the standard FE basis functions ensures that ϕ^h is equal to ϕ at each node. The zero level set of this discretised level set function, $\Gamma^h = \{\mathbf{x} \in \Omega \mid \phi^h(\mathbf{x}) = 0\}$, provides an approximation to Γ .

If a function has a jump in value then we call it a strong discontinuity, and typically step-enrichment,

$$\Psi_{\text{step}} = \text{sign}(\phi^h),$$

is used. Alternatively, if a function is continuous but has a jump in its gradient we call it weakly discontinuous, and typically abs-enrichment,

$$\Psi_{\text{abs}} = |\phi^h|, \quad (2)$$

is used.

The local enrichment functions $\Psi\psi_i$ are constructed using the standard FEM basis (PU) functions ψ_i . They can also be ‘shifted’¹⁹ so that they become zero at each node, thus regaining the Kronecker- δ property of the XFEM approximation. The shifted local step-enrichment functions are

$$\psi_i^* = (\text{sign}(\phi^h) - \text{sign}(\phi_i))\psi_i,$$

and the shifted local abs-enrichment functions are

$$\psi_i^* = (|\phi^h| - |\phi_i|)\psi_i, \quad (3)$$

where $\phi_i = \phi(\mathbf{x}_i)$ and \mathbf{x}_i is the position of the i^{th} global node.

Since the FE basis functions form a PU over Ω , our local enrichment functions are able to exactly reproduce the global enrichment function Ψ on Ω . These enriched basis functions, together with the standard part of the XFEM approximation should allow us to accurately represent any function with a strong or weak discontinuity located at $\phi^{-1}(0)$, but that is smooth elsewhere.

The local finite element basis functions, defined on a reference element $\Omega_{\text{ref}} = [-1, 1]^d \in \mathbb{R}^d$, are the restrictions of the global finite element basis functions. We define the enriched local basis functions in the same way, as the restrictions of the local enrichment functions to each element.

2.1 | Blending

The standard FE basis functions build a PU over the whole domain Ω , allowing the global enrichment function to be reproduced exactly everywhere. Although this is desirable in problems where the enrichment is required globally, the discontinuities we hope to incorporate are local features; elsewhere the solutions are smooth. In elements that contain a discontinuity the local standard basis functions of degree p , together with the corresponding local enriched basis functions, form a complete basis for piecewise polynomial functions of degree p on the reference element. However, in elements that do not contain a discontinuity the global step- and abs-enrichment functions can already be reproduced by the standard finite element basis alone. We therefore apply the enrichment only locally, close to the discontinuity.

Suppose we incorporate only the enriched basis functions that correspond to a subset I^* of nodes. Then we classify elements as follows.

- Definition 1.**
1. Elements over which the standard basis functions corresponding to the nodes I^* form a PU are called *reproducing* elements;
 2. elements over which every standard basis function corresponding to a node in I^* vanishes are called *unenriched* elements; and
 3. elements over which the standard basis functions corresponding to the nodes I^* neither vanish nor form a PU are called *blending* elements.

All nodes belonging to elements cut by the discontinuity belong to I^* , and so the global enrichment function can be reproduced there. In an element that neighbours a reproducing element only some of its nodes belong to I^* . The standard global

basis functions corresponding to those nodes have support in the element, but those basis functions do not form a PU over the element. This element is therefore a blending element and is able to partially, but not fully, reproduce the global enrichment function. This in itself does not present a problem since we are only concerned with reproducing the global enrichment locally in elements that contain a discontinuity. However, the terms introduced into the approximation that do partially reproduce the global enrichment can be problematic. The local abs-enrichment functions corresponding to nodes shared between reproducing and blending elements have support in both elements, but the enriched basis functions are of a higher degree than the standard basis functions. The (parasitic) terms introduced by these nodes into the local approximation in the blending region therefore cannot be removed by contributions from the standard basis functions.

It is expected that an approximation of order p should be able to exactly reproduce functions that are piecewise polynomial of degree p . However, the parasitic terms cause the XFEM approximation to be unable to exactly represent these functions. In some cases, as we will see in section 4.1, It is sometimes possible for the XFEM solution to converge at the optimal rate under mesh refinement despite the inability of the approximation space to exactly represent piecewise polynomial functions²⁰. However, the presence of these parasitic terms generally does adversely affect the achievable rates of convergence. Note that blending is not required when shifted step-enrichment is used because the enrichment vanishes outside of elements that contain the discontinuity.

Since abs-enrichments do suffer from parasitic terms in the blending region, unless these spurious contributions can be eliminated or otherwise accounted for then sub-optimal rates of convergence for the XFEM approximation will result. Several strategies exist to combat these complications in the blending region. These include:

1. a global enrichment strategy where enough additional enrichments at element boundaries are included to eliminate the spurious contributions from neighbouring elements,
2. the use of additional hierarchical basis functions in blending elements⁷,
3. the construction of assumed strain blending elements^{7,14} to eliminate the unwanted terms in the blending region analytically,
4. a strategy in which the reproducing region is uncoupled from the rest of the domain and the solutions are matched to regain continuity^{8,21},
5. the use of partition of unity functions N_i of a lower order in the enriched part of the approximation²² such that the additional terms introduced in the blending region can be represented by the standard FE basis in those elements,
6. a corrected XFEM^{23,24} where a ramp function is employed to reduce the enriched contribution to zero on the outer edge of the blending region,
7. the use of several enrichment terms based on linear partition of unity functions N_i ²⁵, and
8. a modified XFEM²⁶ where the enrichment is constructed such that it vanishes in the blending region.

Strategy 1 takes advantage of the local linear dependence of the local enrichment functions, but introduces many additional unknowns into the system, drastically increasing the cost. In strategy 2 additional degrees of freedom are required, increasing the problem size. This strategy is used with linear elements in Chessa et al.⁷, and extended to higher order in Tarancón et al.²⁷, although the results are not always optimal²⁸. Strategy 3 uses assumed strain projection to eliminate the unwanted terms in the blending elements with analytic representations of the parasitic terms. It performs optimally, and the additional degrees of freedom can be removed via static condensation^{14,29}. However, the equations associated with these unknowns are problem-dependent, meaning that a new assumed strain blending element must be constructed if a different set of equations are to be solved, and the adjustment is quite involved²⁸. Linear assumed strain blending elements are used in Chessa et al.⁷, Legay et al.²² and Gracie et al.¹⁴. The decomposition of the domain into enriched and standard FE regions in strategy 4, with the solution matched between regions by enforcing continuity, is a promising approach. No nodes are shared between the domains, and so the enriched basis functions only have support in the reproducing region. Parasitic terms are therefore not introduced. Due to the matching of enriched and unenriched approximations, strong continuity cannot in general be regained even on conforming meshes. Instead weak continuity must be recovered, and this can be done in several ways including pointwise matching at nodes (Laborde et al.⁸), a discontinuous Galerkin method (Gracie et al.¹⁴), Lagrange multipliers (e.g. the mortar method as in Chahine et al.³⁰), the penalty method or Nitsche's method^{31,32}.

Strategies 6 and 8 both localise the enrichment by changing the global enrichment function such that it vanishes away from the discontinuity. The corrected XFEM requires additional nodes to be enriched such that the basis functions build a PU over the blending region in addition to the reproducing region. The use of the ramp function prevents spurious contributions from entering the unenriched region. The modified XFEM is discussed in detail in section 2.3.

2.2 | Optimal Convergence

Error bounds on generalised/unfitted finite element approximations of $O(h^p)$ in the H^1 norm and $O(h^{p+1})$ in the L^2 norm are proved by Babuška et al.³³ and Lehrenfeld and Reusken³⁴, although numerical results demonstrating these rates of convergence are not presented.

For a point interface, in one dimension, optimal rates of convergence for a weak discontinuity have been demonstrated by Fries²³ for approximations up to $p = 4$.

Fries and Belytschko²⁸ note that the description of an interface in higher dimensions is formally independent of the approximation in the bulk. Interfaces are often assumed to be (piecewise) planar in order to simplify the quadrature²⁸. Higher order convergence studies with planar cracks by Laborde et al.⁸ and Tarancón et al.²⁷ have displayed optimal accuracy. However, to obtain optimal convergence rates for the solution to problems involving curved interfaces a higher order description of both the approximation and the interface is required, as demonstrated by Cheng and Fries²⁵ and others. It is also essential to resolve problems in the blending elements, as discussed in the previous section.

Higher order descriptions of the interface in the XFEM have been considered, for example in Dolbow et al.³⁵, Stazi et al.³⁶ and Zi and Belytschko³⁷, but in these papers the interface is still considered to be straight for the purposes of integration²⁸. As such, optimal convergence is not obtained. Some recent work has focused on discretising curved interfaces to the required accuracy using piecewise linear approximations of the within elements (Jiang et al.³⁸), or by using higher order level set functions (Fries and Omerović³⁹). Other approaches involve local remeshing about the interface and the use of standard finite elements^{40,41}, or local refinement about the interface^{42,43}. There has also been some work on improving the split integration in cells containing the interface^{43,39,44}. In Ndeffo et al.⁴⁵, the approximation space is modified to improve conditioning, but optimal convergence is not obtained.

Optimal convergence results have been achieved for straight strong discontinuities in^{22,27,46} (and in⁸ where blending strategy 4 was used around crack tips), and for straight weak discontinuities (for $p \leq 4$) in²² using strategy 5. Optimal convergence results for curved strong discontinuities are presented in⁴⁷. However, achieving optimal convergence rates for curved weak discontinuities is not as straightforward.

Cheng and Fries²⁵ show that strategies 5 and 8 converge sub-optimally for curved weak discontinuities with approximations of order $p > 1$. They go on to achieve “close to optimal” rates of convergence for curved weak discontinuities using strategies 6 and 7 with approximations of order $p \leq 3$, although the latter suffered from ill-conditioning.

These studies considered only quadratic and cubic approximations. Until recently, truly high-order ($p > 3$) XFEM had not been reported in the literature. Byfut and Schröder⁴⁶ have since developed a high-order XFEM for polygonal crack problems, reporting optimal rates of convergence for orders $p \leq 4$. As-yet there have been no truly optimally-convergent higher order strategies for curved weak discontinuities reported in the literature. Furthermore, there have been no optimal convergence results presented for blending strategy 8 for weak discontinuities, straight or curved, for approximations of order $p > 1$. We now take a closer look at strategy 8, the so-called modified XFEM.

2.3 | The Modified XFEM

The problems that arise in the blending region occur because some of the abs-enriched global basis functions have support outside of the reproducing region, in the blending region. The modified XFEM, introduced by Moës et al.²⁶, alters the global abs-enrichment function in order to avoid these problems. It uses a modified global enrichment function,

$$\Psi_{\text{modified}} = |\phi^h| - |\phi|^h, \quad (4)$$

where we define $|\phi|^h = \sum_i |\phi_i| \psi_i$. Note that here we have chosen the opposite sign from that used in²⁶. The first term in this global enrichment is the same as for the standard shifted abs-enrichment, and has a jump in the gradient at $(\phi^h)^{-1}(0)$. The second term is just the standard finite element representation of the absolute value of the level set function, $|\phi|$. The modified local

enriched basis functions are

$$\psi_i^{\text{mod}} = (|\phi^h| - |\phi|^h)\psi_i. \quad (5)$$

Now, in elements not cut by the discontinuity the sign of ϕ does not change. Therefore $|\phi^h| = |\phi|^h$, and so the enrichment vanishes. Thus parasitic terms are not introduced to the approximation in the blending elements. The construction of the modified global enrichment function is shown in figure 1

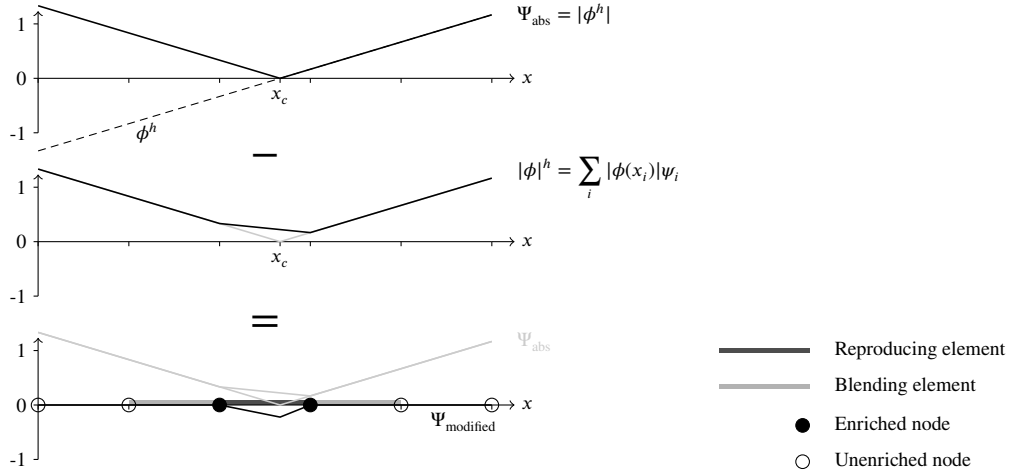


FIGURE 1 Construction of the modified global enrichment functions using linear PU functions. (Based on figure 14 from²⁵.)

This approach has several advantages over other blending methods. Firstly, in the modified XFEM only the nodes in the reproducing elements are enriched, whereas in the corrected XFEM (and others) the nodes in the blending region are also enriched. The modified XFEM therefore requires fewer degrees of freedom than other blending techniques, although often the affect of this on the total problem size is small. Secondly, in order to construct the local enrichment functions it is necessary to compute the level set function everywhere that they have support. For the standard/corrected local enrichment functions this is over both the reproducing and blending regions, whereas for the modified local enrichment functions it is just on the reproducing region. The initialisation and update of the level set function can be costly^{48,49}, so it is advantageous that the modified XFEM allows the level set function to be calculated on a narrower band around the discontinuity. However, it is often necessary to calculate the level set function on a wider band for other reasons, such as for velocity extension or for updates to fast-moving interfaces. Additionally, because ϕ^h matches ϕ at each node, we have $\psi_i^{\text{mod}}(x_j) = 0$ for all i, j and so the approximation naturally has the Kronecker- δ property: no further shifting is required.

However, as reported in²⁵, the modified XFEM is known to yield poor rates of convergence for higher order approximations. This problem must be addressed before the method can be used efficiently at higher orders. We consider this in more detail in section 4.2.

3 | A POISSON PROBLEM WITH A DISCONTINUITY

Let us now introduce a discontinuous problem to which we can apply the XFEM. We will use it in the following sections to analyse the performance of different enrichments. Consider a Poisson problem that includes a spatially varying diffusivity $D = \text{diag}(\boldsymbol{\mu}(\mathbf{x}))$, with $\boldsymbol{\mu}(\mathbf{x}) > \mathbf{0}$. That is,

$$\nabla \cdot (D\nabla u) = f. \quad (6)$$

If $\boldsymbol{\mu}$ is discontinuous then the solution u will also be discontinuous. We impose boundary conditions

$$u|_{\partial\Omega} = u_D. \quad (7)$$

We write the Galerkin weak form of (6) as

$$\begin{aligned} \int_{\Omega} (\nabla \cdot (D\nabla u) - f)v \, d\Omega &= 0 \\ \int_{\Omega} D\nabla u \cdot \nabla v + f v \, d\Omega - \int_{\partial\Omega} D\nabla u \hat{\mathbf{n}} \cdot \mathbf{s} \, ds &= 0 \quad \forall v \in V. \end{aligned} \quad (8)$$

We restrict the trial space to functions which satisfy the boundary conditions (7), $H_D^1(\Omega) \subset H^1(\Omega)$. We can also restrict our test space to functions which vanish at the boundary, $H_0^1(\Omega) \subset H^1(\Omega)$. The weak form now becomes

$$\text{find } u \in H_D^1(\Omega) \quad \text{s.t.} \quad \int_{\Omega} D\nabla u \cdot \nabla v + f v \, d\Omega = 0 \quad \forall v \in H_0^1(\Omega). \quad (9)$$

We discretise the test and trial spaces, $H_D^h(\Omega), H_0^h(\Omega) \subset H^1(\Omega)$, and then choose a basis $H^h(\Omega) = \text{span}\{\psi_i, \psi_i^*\}$, where ψ_i are the standard finite element basis functions of degree p and ψ_i^* are local enrichment functions based on the global abs-enrichment (or one of its variants) and constructed using the ψ_i . We relabel this basis using the functions $\{\zeta_k\} = \{\psi_i, \psi_i^*\}$ with corresponding unknowns $\{u_k\}$. Boundary conditions may be imposed by fixing values for the unknowns corresponding to basis functions that are nonzero at the boundary. We write the XFEM approximation as

$$u^{\text{XFEM}} = \sum_i u_i \psi_i + \sum_i u_i^* \psi_i^* = \sum_k u_k \zeta_k.$$

This gives the discrete weak form

$$\text{find } \{u_j \in \mathbb{R}\}_{j=1}^M \quad \text{s.t.} \quad \int_{\Omega} D \sum_{j=1}^{2N} u_j \nabla \zeta_j \cdot \nabla \zeta_k + f \zeta_k \, d\Omega = 0, \quad k = 1, \dots, M,$$

where N is the global number of nodes, $2N$ is the number of global basis functions, and $M \leq 2N$ is the number of degrees of freedom in the problem. This is a system of M linear algebraic equations in M unknowns and can be solved using Newton's method. The entries in the residual vector and Jacobian matrix are

$$r_k = \int_{\Omega} D \sum_{j=1}^{2N} u_j \nabla \zeta_j \cdot \nabla \zeta_k + f \zeta_k \, d\Omega \quad (10)$$

and

$$J_{kj} = \int_{\Omega} D \nabla \zeta_j \cdot \nabla \zeta_k \, d\Omega.$$

3.1 | Tools for Error Analysis

In order to compare the quality of different approximations we must be able to measure how well they match the function we are trying to approximate. A measure of the quality of an approximation is the size of the error $\varepsilon = u - u^h$ between the exact solution u and the FE approximation u^h . We define norms on $L^2(\Omega)$ and $H^k(\Omega)$ to be

$$\|g\| = \left(\int_{\Omega} g^2 \, d\Omega \right)^{\frac{1}{2}}, \quad g \in L^2(\Omega), \quad (11)$$

and

$$\|g\|_k = \left(\int_{\Omega} \sum_{i=0}^k \sum_{j=0}^d \left(\frac{\partial^i g}{\partial x_j^i} \right)^2 \, d\Omega \right)^{\frac{1}{2}}, \quad g \in H^k(\Omega), \quad (12)$$

respectively, for $\Omega \subset \mathbb{R}^d$. If D is sufficiently smooth, then a bound on the error of the finite element approximation to (9),

$$\|\varepsilon\|_1 \leq C h^{\mu-1} p^{-(k-1)} \|u\|_k, \quad (13)$$

can be obtained where $\mu = \min(k, p + 1)$ and C is independent of h, p and u but does depend on $k^{3,50}$. We also assume that the forcing $f \in H^k(\Omega)$ so that it does not appear in the error estimate. Note that for sufficiently smooth problems the upper

bound on the error in the approximation takes the form h^p . Uniform h -refinement should therefore lead to polynomial rates of convergence whereas p -refinement should lead to exponential rates of convergence.

It is often more convenient to compute these errors using a different norm. The weak form (9) of the Poisson problem defines an inner product

$$\langle u, v \rangle = \int_{\Omega} D \nabla u \cdot \nabla v \, d\Omega$$

on $H^1(\Omega)$. We can use this to define an energy norm

$$\|g\|_E = \langle g, g \rangle^{\frac{1}{2}} = \left[\int_{\Omega} D \nabla g \cdot \nabla g \, d\Omega \right]^{\frac{1}{2}}, \quad g \in H^1(\Omega).$$

This energy norm is equivalent to the $H^1(\Omega)$ norm⁵⁰, and we will use it in place of the H^1 norm to calculate our error estimates.

3.2 | Numerical Integration of Discontinuous Functions

We evaluate the integrals (10) numerically. However, the integrand may be discontinuous on the interior of an element so we must take care to evaluate these integrals correctly. Using standard Gauss-type quadrature rules⁵¹ poorly approximates such integrals, and this can seriously affect the accuracy of XFEM solutions.

Instead we use split integration^{11,19,52}, or subcell quadrature, to accurately evaluate such integrals. We can decompose an element Ω^e into subelements Ω_i^e such that $\bigcup_i \Omega_i^e = \Omega^e$, $\bigcap_i \Omega_i^e = \emptyset$. Since $\int_{\Omega^e} f = \sum_i \int_{\Omega_i^e} f$, this decomposition does not affect the value of the analytic integral. However, if we can choose a decomposition such that the integrand f is smooth on each subelement then standard Gauss-type quadrature can be used on each part and so the discontinuous integral can be approximated accurately. The subelements are used simply for the integration so they need not conform, and they introduce no new unknowns into the problem. The only additional cost is in their construction and the need for quadrature to be performed over the additional subelements.

Note that for quadrilateral elements the isoparametric mapping of the quadrature knot points of the reference element loses the exact integration property^{53,54}, but results can still be very good²⁸ and need not affect the overall rate of convergence of the method as we will see.

Element decompositions into subelements that align with the discontinuity are employed widely in the XFEM²⁸. For elements Ω^e that are cut horizontally by a discontinuity Γ at height $t^* \in \mathbb{R}$, we can write the location of Γ as $\Gamma = \{(s, t^*) \mid s \in [-1, 1]\}$. Then we can divide Ω^e about Γ into two subelements $\Omega_1^e = [-1, 1] \times [t^*, 1]$ and $\Omega_2^e = [-1, 1] \times [-1, t^*]$. The integrand is smooth inside each subelement and so we apply a standard Gauss-type quadrature rule on each. This scheme is used in section 4. It is extended for arbitrary discontinuities in section 5, and then used again in section 6.

4 | A STRAIGHT WEAK DISCONTINUITY

We now consider the discontinuous Poisson problem (6) in two spatial dimensions with a straight weak discontinuity. Later (in section 5) we extend this problem by considering a curved discontinuity. This problem serves to separate the complications relating to the curvature of the discontinuity from those that arise from the presence of the discontinuity itself. We specify that the diffusivity varies only in the y -direction by setting $\boldsymbol{\mu} = (1, \mu)^T$. Equation (6) now becomes

$$\frac{\partial^2 u}{\partial x^2} + \frac{\partial}{\partial y} \left(\mu \frac{\partial u}{\partial y} \right) = f, \quad (14)$$

on the domain $(x, y) \in \Omega = [0, 1]^2$. We specify boundary conditions

$$u \Big|_{x=0} = u \Big|_{x=1} = u \Big|_{y=0} = 0 \quad \text{and} \quad u \Big|_{y=1} = \sin(\pi x),$$

and choose forcing $f = 0$ and diffusivity such that

$$\mu(y) = \begin{cases} \mu_1, & y \leq y_c, \\ \mu_2, & y > y_c, \end{cases}$$

$\mu_1, \mu_2 > 0$. The analytic solution is then

$$u(x, y) = \begin{cases} \sin(\pi x)A_1(e^{\eta_1 y} - e^{-\eta_1 y}), & y \leq y_c, \\ \sin(\pi x) [A_2(e^{\eta_2 y} - e^{\eta_2(2-y)}) + e^{\eta_2(1-y)}], & y > y_c. \end{cases}$$

Details can be found in⁵⁵. Let us choose $\mu_1 = 1$, $\mu_2 = 10$ and $y_c = \frac{2}{3}$ so that there is a discontinuity in the gradient of the solution at $y = \frac{2}{3}$. The exact solution is shown in figure 2

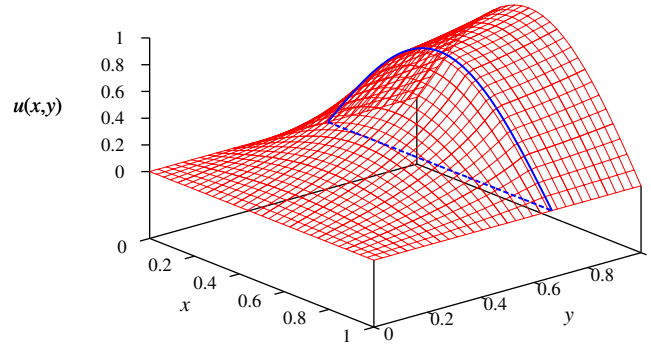


FIGURE 2 Exact solution to the two-dimensional Poisson problem (14) with discontinuous gradient at $y = \frac{2}{3}$.

4.1 | Higher Order Approximation

We solve the two-dimensional discontinuous Poisson problem (14) (details in²⁰) and use an initial 4×4 mesh of bilinear elements and then uniformly h - and p -refine it to the appropriate level. With the discontinuity located at $y = \frac{2}{3}$ it can never align with an element boundary at any refinement level, thus ensuring the discontinuity always cuts element interiors. Figure 3 shows the L^2 error for the corrected XFEM and modified XFEM solutions on the resulting mesh.

The modified XFEM gives optimal convergence for approximations of orders $p = 1$, but only sub-optimal convergence for orders $p \geq 2$. Increasing the order of approximation does not improve the rate of convergence for $p > 1$: all approximations converge at a rate no faster than $O(h^{5/2})$ in the L^2 norm. This demonstrates the poor rates of convergence that can be achieved for higher order modified XFEM approximations, as discussed in section 2.3.

In fact, the modified XFEM approximation space does not span the space of piecewise quadratic functions²⁰. That is, there are piecewise quadratic functions that cannot be represented exactly by any combination of modified XFEM basis functions, and so the Galerkin approximation to such problems fails to converge optimally²⁰.

4.2 | Corrections to the Modified XFEM

Both the shifted abs-enrichment (with appropriate global enrichment) and the corrected XFEM are able to achieve optimal rates of convergence for discontinuous problems. To understand why the modified XFEM converges suboptimally we look at how it differs from those XFEMs that do recover optimal rates of convergence.

The structure of the modified abs-enrichment (4) is similar to that of the shifted abs-enrichment (2). The shifting of the local abs-enriched basis functions is performed by subtracting a constant contribution $|\phi_j|$ from the global abs-enrichment function before multiplication by the local basis functions of the standard FEM. In contrast, the modified local basis functions are constructed by subtracting the whole FE representation of the absolute value of the level set function $|\phi|^h = \sum_j |\phi_j| \psi_j$, from the global abs-enrichment. That is, shifted abs-enrichment subtracts a polynomial of degree zero from the global enrichment whereas modified abs-enrichment subtracts a polynomial of degree at most p . Multiplication by the appropriate standard FE basis function then gives the corresponding local enrichment function. Let us define the smooth and discontinuous parts of a function f using a decomposition of the form

$$f(x) \equiv a(x)|\phi(x)| + b(x), \quad (15)$$

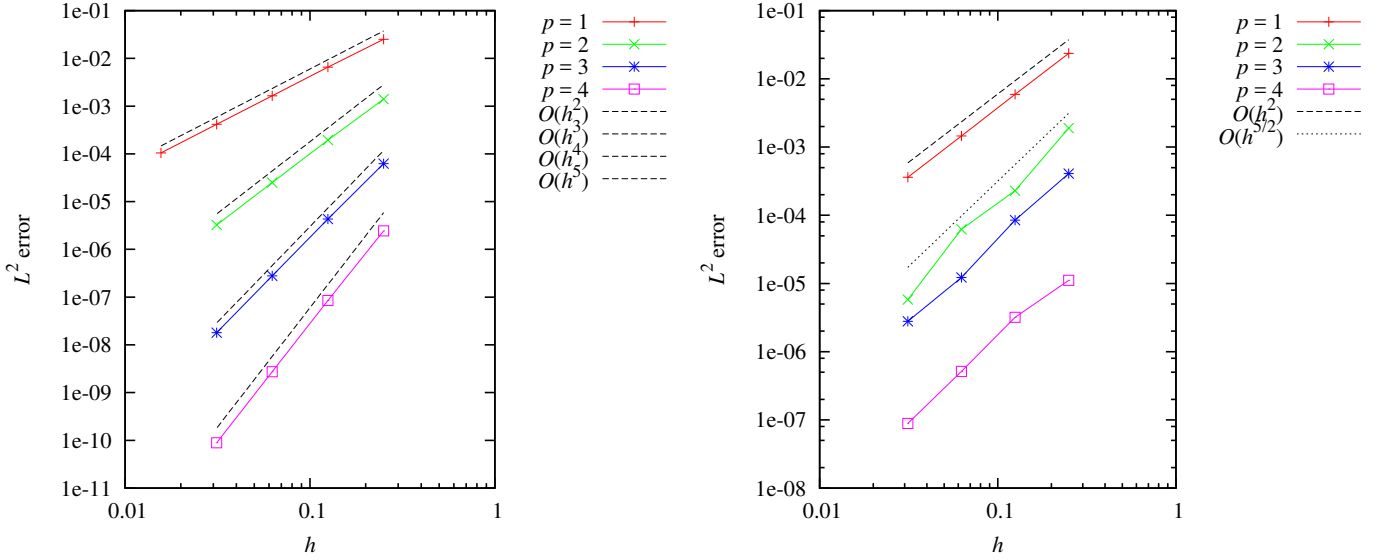


FIGURE 3 Convergence results in the L^2 norm for corrected XFEM (left) and modified XFEM (right) approximations up to order $p = 4$. The modified XFEM approximation only converges optimally for the linear approximation. For orders $p > 1$ the rate of convergence is no better than $O(h^{5/2})$.

with a, b polynomials. We call b the smooth part and $a|\phi|$ the discontinuous part. Now, we may decompose the local enrichment functions into their smooth and discontinuous components using $\psi_i^* \equiv (a_i|\phi| + b_i)\psi_i$, where a_i and b_i are polynomials in x . For both the shifted abs-enrichment and the modified abs-enrichment we have $a_i \equiv 1$. The discontinuous parts of the local enrichment functions therefore have degree $\deg(|\phi|\psi_i) = 2p$. However, for the shifted abs-enrichment $b_i \equiv -|\phi|$, whereas for the modified abs-enrichment $b_i \equiv -|\phi|^h$. The smooth parts of the shifted and modified local enrichment functions have degree $\deg(|\phi|\psi_i) = p$ and $\deg(|\phi|^h\psi_i) = 2p$ respectively.

Let us also decompose the exact solution, u , and the XFEM approximation, u^{XFEM} , into their smooth and discontinuous parts. That is,

$$u = \alpha|\phi| + \beta,$$

where α, β are polynomials in x , and

$$u^{\text{XFEM}} = \sum_i u_i \psi_i + \sum_i u_i^* (a_i|\phi| + b_i)\psi_i = \left[\sum_i u_i^* a_i \psi_i \right] |\phi| + \sum_i (u_i + u_i^* b_i)\psi_i.$$

The ability of the XFEM approximation to accurately represent u depends on the ability of the smooth and discontinuous parts of the approximation to represent the corresponding parts of the exact solution. Notice that the coefficient u_i^* appears in both the smooth and discontinuous parts of the approximation, and so they cannot be approximated independently. A change to the enriched unknown affects both parts of the approximation. We will see in the following example how this property, combined with the structure of the different XFEM enrichments, is the cause of suboptimal rates of convergence attainable using the modified XFEM.

We expect that an XFEM approximation constructed from standard basis functions of degree p should exactly reproduce piecewise polynomial functions of degree p of the form (15). In the following example we demonstrate how the shifted abs-enrichment is able to exactly represent such functions whereas the modified XFEM is not.

Example 1. Let us suppose that there is an exact representation $u^{\text{XFEM}} \equiv u$, and so $\alpha = \sum_i u_i^* a_i \psi_i$ and $\beta = \sum_i (u_i + u_i^* b_i)\psi_i$. Suppose the level set function has $\deg(\phi) = p_\phi$. Then u is piecewise of degree p if $\deg(\alpha) = p - p_\phi$ and $\deg(\beta) = p$. Now suppose we perturb u by adding a function $\Delta\alpha|\phi|$, $\deg(\Delta\alpha) = \deg(\alpha)$. This gives a new function $\hat{u} = \hat{\alpha}|\phi| + \beta$, where $\hat{\alpha} = \alpha + \Delta\alpha$, $\deg(\hat{\alpha}) = p - p_\phi$. This ensures that \hat{u} is also piecewise polynomial of degree p . It should therefore also be representable exactly

using the XFEM basis functions. Let us write our XFEM approximation to this perturbed function as

$$\hat{u}^{\text{XFEM}} = \left[\sum_i \hat{u}_i^* a_i \psi_i \right] |\phi| + \sum_i (\hat{u}_i + \hat{u}_i^* b_i) \psi_i. \quad (16)$$

Since $\deg(\Delta\alpha) < p$ we can express it as a linear combination of the standard basis functions,

$$\Delta\alpha = \sum_i \Delta\alpha_i \psi_i,$$

with coefficients $\Delta\alpha_i \in \mathbb{R}$. Matching the discontinuous parts of \hat{u}^{XFEM} and \hat{u} gives

$$\sum_i \hat{u}_i^* a_i \psi_i = \sum_i (u_i^* a_i + \Delta\alpha_i) \psi_i.$$

So for the XFEM approximation to be exact we require $\hat{u}_i^* = u_i^* + \Delta\alpha_i/a_i$. Substituting this into equation (16) gives

$$\hat{u}^{\text{XFEM}} = \underbrace{\left[\sum_i (u_i^* a_i + \Delta\alpha_i) \psi_i \right]}_{\hat{\alpha}} |\phi| + \underbrace{\sum_i (\hat{u}_i + (u_i^* + \Delta\alpha_i/a_i) b_i) \psi_i}_{\hat{\beta}}.$$

We determine \hat{u}_i by matching the continuous parts of \hat{u}^{XFEM} and \hat{u} , $\hat{\beta} = \beta$. That is,

$$\begin{aligned} \sum_i (\hat{u}_i + \Delta\alpha_i b_i/a_i + u_i^* b_i) \psi_i &= \sum_i (u_i + u_i^* b_i) \psi_i \\ \sum_i (\hat{u}_i - u_i + \Delta\alpha_i b_i/a_i) \psi_i &= 0. \end{aligned} \quad (17)$$

If we use the shifted abs-enriched local basis functions in the XFEM approximation then $a_i = 1$ and $b_i = -|\phi_i|$. Writing our perturbed enriched unknowns as

$$\hat{u}_i = u_i + \Delta\alpha |\phi_i| \quad (18)$$

satisfies equation (17). Thus given an exact representation u^{XFEM} of u we have found expressions for the unknowns \hat{u}_i , \hat{u}_i^* such that \hat{u}^{XFEM} exactly matches the perturbed function \hat{u} .

If we use the modified XFEM basis functions instead then $a_i = 1$ and $b_i = -|\phi|^h$. Equation (17) becomes

$$\begin{aligned} \sum_i (\hat{u}_i - u_i - \Delta\alpha_i |\phi|^h) \psi_i &= 0 \\ \left[\sum_i (\hat{u}_i - u_i) \psi_i \right] - \Delta\alpha |\phi|^h &= 0. \end{aligned}$$

The first term is a polynomial of degree p , whereas the second term has degree $\deg(\Delta\alpha) + \deg(|\phi|^h) = (p - p_\phi) + p = 2p - p_\phi$. If the degree of the level set function, p_ϕ , is less than p then it is not possible to find expressions for the perturbed unknowns that satisfy the equality. The smooth part of the XFEM approximation is not equal to that of the perturbed exact solution, so it is therefore impossible to exactly represent the perturbed solution \hat{u} using the modified XFEM¹.

Now, consider the linear case with $p = 1$. The level set function must have degree $p_\phi = 1$, and so for u to be piecewise linear we must have $\deg(\alpha) = \deg(\Delta\alpha) = p - p_\phi = 0$. This implies $\Delta\alpha_i = \Delta\alpha$ for all i . We express $|\phi|^h$ as a linear combination of the standard basis functions, $|\phi|^h = \sum_i |\phi_i| \psi_i$, and so equation (17) becomes

$$\sum_i (\hat{u}_i - u_i - \Delta\alpha |\phi_i| \psi_i) \psi_i = 0.$$

The expression (18) for the perturbed unknowns again satisfies the equation. In this case the XFEM approximation \hat{u}^{XFEM} for the piecewise linear function \hat{u} is exact, and so the modified XFEM enriched basis functions constructed from linear PU functions escape the problems suffered at higher orders. This explains why the modified XFEM recovers optimal rates of convergence in the linear case, but not for higher order approximations.

This example demonstrates the inability of the modified XFEM approximation to accurately represent the smooth and discontinuous parts of the solution independently. Higher order terms resulting from the construction of the modified XFEM basis

¹Note that, in general, this does not imply that using a level set function with degree p ensures that the modified XFEM approximation is exact for any piecewise polynomial of degree p . The class of functions for which $u = \alpha|\phi| + \beta$ with $\deg(\alpha) = 0$, $\deg(\beta) \leq p$ and $\deg(\phi) = p$ is much smaller.

functions appear in the smooth part of the approximation and cannot be eliminated by the standard FE basis functions. This is similar to the problems with blending encountered with the original abs-enrichment, except that rather than the spurious terms appearing in the approximation in the blending region, here they appear in the reproducing region instead. If we are to recover optimal rates of convergence for modified XFEM approximations then we must eliminate these higher order contributions, of degree $p + 1, \dots, 2p$, to the smooth part of the approximation.

4.2.1 | Construction of Correction Polynomials

Let us consider the difference between the local basis functions of the shifted abs-enrichment and the modified abs-enrichment on the reference element $[-1, 1] \subset \mathbb{R}$. Let ψ_i^{abs} denote the local enriched basis functions of the shifted abs-enrichment and ψ_i^{mod} denote those of the modified abs-enrichment.

Now consider the XFEM approximation computed using the shifted abs-enriched basis functions,

$$u^{\text{abs}} = \sum_i u_i \psi_i + \sum_i u_i^* \psi_i^{\text{abs}}. \quad (19)$$

Let us fix the values of the standard and enriched unknowns and substitute the modified XFEM basis functions into (19) in place of the shifted abs-enriched basis functions. The new approximation is

$$u^{\text{mod}} = \sum_i u_i \psi_i + \sum_i u_i^* \psi_i^{\text{mod}}.$$

The difference between these two approximations is

$$u^{\text{mod}} - u^{\text{abs}} = \left[\sum_i u_i \psi_i + \sum_i u_i^* \psi_i^{\text{mod}} \right] - \left[\sum_i u_i \psi_i + \sum_i u_i^* \psi_i^{\text{abs}} \right] = \sum_i u_i^* d_i,$$

where

$$d_i = \psi_i^{\text{mod}} - \psi_i^{\text{abs}} = \psi_i \left(|\phi_i| - \sum_j |\phi_j| \psi_j \right). \quad (20)$$

Note that d_i is a polynomial of degree $2p$ on each element, and that the discontinuity is not present. Thus the difference $u^{\text{mod}} - u^{\text{abs}}$ is also piecewise of degree $2p$. Therefore, given an XFEM solution computed using the shifted XFEM (everywhere), if we were to substitute in the basis functions of the modified XFEM in place of those of the shifted XFEM then we would have the same description of the discontinuity, but with an additional polynomial contribution of degree at most $2p$ on each element. If we can remove this contribution then we should be able to recover the same optimal rates of convergence for modified XFEM approximations as for shifted abs-enrichments. However, we must do this only in the reproducing region because otherwise we would lose the property that the enrichment vanishes everywhere else.

We project the basis functions into a hierarchical basis for polynomials of degree at most $2p$. This yields correction polynomials in terms of that basis, and allows contributions at certain orders to be removed in a straightforward fashion.

We define a one-dimensional modal basis $\{m_i\}_{i=0}^q$ of order q on $s \in [-1, 1]$ as

$$m_i(s) = \begin{cases} \frac{1}{2}(1-s), & i = 0, \\ \frac{1}{2}(1+s), & i = 1, \\ \frac{1}{4}(1-s)(1+s)P_{i-2}(s), & 2 \leq i \leq q, \end{cases} \quad (21)$$

where P_n is the n^{th} Legendre polynomial⁵¹. For $n \geq 2$, $\deg(P_n) = n$. Higher-dimensional modal bases of order q , $\{M_j(\mathbf{s})\}_{j=0}^{(q+1)^d-1}$, can be defined as tensor products of the one-dimensional basis functions on $[-1, 1]^d$. We project the differences d_i (polynomials of degree $2p$) into this modal basis $\{M_j\}$ up to order $2p$ to produce a system of $(2p+1)^d$ equations and unknowns,

$$A^{(i)} \xi^{(i)} = f^{(i)}. \quad (22)$$

This system is then solved to find the unknowns $\xi_j^{(i)}$. We remove the contributions to the modified enriched basis functions at orders $p+1 \leq q < 2p$ by subtracting the corresponding terms $\xi_j^{(i)} M_j(\mathbf{s})$ ²⁰. Note that $\xi_j^{(i)}$ can be expressed purely in terms of the values ϕ_i of the level set function at the element nodes, and that these are known a priori.

We solved the system (22) symbolically using Mathematica⁵⁶, just once, to find expressions for the correction polynomials in terms of the values of the level set function at the nodes. The evaluation of these polynomials at runtime is fast, and so the cost of evaluating an enriched basis function in this way is comparable to that of evaluating an enriched basis function of the

corrected or abs-enriched XFEMs. The additional cost of calculation of the modified XFEM basis functions is only the few extra floating point operations required to evaluate the correction polynomials from their analytic expressions.

Contributions of degree 3 are removed from the XFEM approximation by subtracting a correction polynomial C_i^3 of degree 3 of the form $C_i^3(s) = \xi_3^{(i)} M_3(s)$ from ψ_i^{mod} . Contributions of degree 4 may be eliminated in a similar way using $C_i^4(s) = \xi_4^{(i)} M_4(s)$. The improved basis functions of order 2 of the modified XFEM are therefore $\psi_i^* = \psi_i^{\text{mod}} - C_i^3 - C_i^4$. The one-dimensional corrections C_i^3 and C_i^4 to the modified enriched basis functions of order 2, written out in full, are:

$$\begin{aligned} C_0^3(s) &= 2(|\phi(s_0)| - |\phi(s_1)|)M_3(s), & C_0^4(s) &= -\frac{2}{3}(|\phi(s_0)| - 2|\phi(s_1)| + |\phi(s_2)|)M_4(s), \\ C_1^3(s) &= 2(-|\phi(s_0)| + |\phi(s_2)|)M_3(s), & C_1^4(s) &= \frac{4}{3}(|\phi(s_0)| - 2|\phi(s_1)| + |\phi(s_2)|)M_4(s), \\ C_2^3(s) &= 2(|\phi(s_1)| - |\phi(s_2)|)M_3(s), & C_2^4(s) &= -\frac{2}{3}(|\phi(s_0)| - 2|\phi(s_1)| + |\phi(s_2)|)M_4(s), \end{aligned}$$

where s_i are the positions of the element nodes. Notice that each correction polynomial vanishes at $s = \pm 1$ (from the definition of the one-dimensional modal basis functions (21)). This ensures that the improved basis functions match the original modified XFEM basis functions at one-dimensional element boundaries, and thus ensures continuity of the global enrichment functions. This is important since the correction polynomials are applied only in the reproducing region. Ensuring continuity across higher-dimensional element boundaries is discussed in section 5.2.

Note also that the only information required for the calculation of these correction polynomials on any element is the standard basis functions on that element and the values of the level set function at its nodes.

The general form of the improved modified XFEM basis functions is

$$\psi_i^* = \psi_i^{\text{mod}} - \sum_{k=p+1}^{2p} C_i^k. \quad (23)$$

Note that we could calculate and subtract other correction polynomials of degree lower than $p+1$, but the XFEM basis functions would still span the same approximation space. Note also that the degree of the local enriched basis function ψ_i^* remains $2p$. We are not simply removing the higher order parts of the modified local enrichment functions.

4.3 | Error Analysis

The rates of convergence of the L^2 and energy errors in the XFEM solution for the improved modified enriched basis functions are shown in figure 4 and table 1. We see that application of the correction polynomials to the modified XFEM local enriched basis functions has allowed us to recover the optimal $O(h^{p+1})$ rates of convergence for the discontinuous Poisson problem (14).

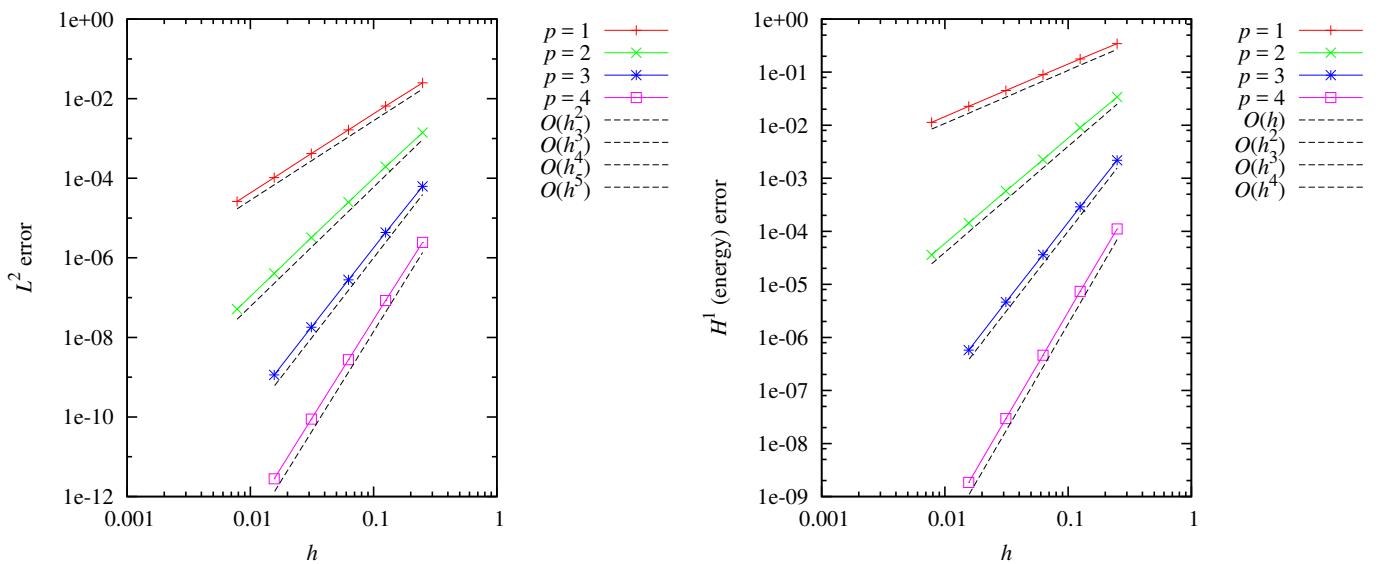


FIGURE 4 Rates of convergence in the L^2 (left) and energy (right) norms for the Poisson problem with a horizontal discontinuity using our improved modified XFEM basis functions for approximations up to order $p = 4$.

TABLE 1 Rates of convergence for the Poisson problem (6) in two dimensions with a straight discontinuity.

p	1	2	3	4
L^2	2.00	2.99	3.97	4.97
H^1 (Energy)	1.00	2.00	2.98	3.98

Note that this elimination of the unwanted additional terms in the enriched approximation space is similar to the assumed/enhanced strain projection methods from ^{7,22,14}, except that the correction is applied to the elements that are cut by the discontinuity rather than to the blending elements, and also that the correction polynomials may be computed a priori rather than requiring additional unknowns to be incorporated into the problem. This is a considerable advantage because it minimises the cost of constructing the enriched basis functions at runtime. Unlike the assumed strain projection methods the resulting corrections are independent of the equations to be solved, so the same enriched basis functions can be used to solve different problems. The assumed/enhanced strain methods achieve optimal convergence for linear PU functions ⁷, but have not yet been applied to higher order approximations.

5 | A CURVED WEAK DISCONTINUITY

Let us now extend our method to allow for curved discontinuities. These present several new challenges in addition to those faced for straight discontinuities in two dimensions. In the previous section we could exactly represent both the level set function and its zero level set using their FE representations. In general, this is no longer the case with curved discontinuities. However, in this section we consider a problem with a curved discontinuity in which the level set function and its zero level set can still be represented exactly. A more general curved interface where this is not the case is considered later in section 6. Here we focus on how the correction polynomials and split integration schemes are affected by interface curvature without introducing errors related to interface location into the approximation.

Consider a Poisson problem similar to (14) but with the diffusivity acting in both directions. We set $\boldsymbol{\mu} = (\mu, \mu)^T$, and so the equation we must solve is

$$\nabla \cdot (\boldsymbol{\mu} \nabla u) = f. \quad (24)$$

We choose a diffusivity such that

$$\mu(x, y) = \begin{cases} \mu_1, & y \leq y_c + vx^\alpha, \\ \mu_2, & y > y_c + vx^\alpha, \end{cases}$$

with a curved discontinuity along the line $y = y_c + vx^\alpha$. In order to provide the exact solution,

$$u(x, y) = \frac{1}{\pi^2 \mu} \sin(\pi(y - (y_c + vx^\alpha))) \sin(\pi x), \quad (25)$$

we require a forcing

$$f(x, y) = -(2 + (\alpha vx^{\alpha-1})^2) \sin(\pi(y - (y_c + vx^\alpha))) \sin(\pi x) - 2\alpha vx^{\alpha-1} \cos(\pi(y - (y_c + vx^\alpha))) \cos(\pi x) - \frac{\alpha(\alpha - 1)vx^{\alpha-2}}{\pi} \cos(\pi(y - (y_c + vx^\alpha))) \sin(\pi x).$$

Figure 5 shows the exact solution (25) to this problem.

Let us start by considering a quadratically curved discontinuity, with $\alpha = 2$, so that we can construct a level set function ϕ whose zero level set is exactly quadratic in x for approximations of order $p \geq 2$. This ensures that the explicit representation of the discontinuity is exact for $p \geq 2$. We have chosen $\phi(x, y) = y - y_c - vx^\alpha$. This function has gradient $\|\nabla \phi\| = \sqrt{1 + (\alpha vx^{\alpha-1})^2}$, and so for powers $\alpha \neq 0$ with $v \neq 0$ it is not a signed distance. Using a signed distance is not a requirement of the method, and we will see that using a level set function without the signed distance property still allows optimal rates of convergence to be achieved. We chose this function because it removes errors in the position of the implicit interface from the approximation.

5.1 | Split Integration in Two Dimensions for Curved Discontinuities

We now generalise the integration scheme used in section 4 to allow for curved discontinuities.

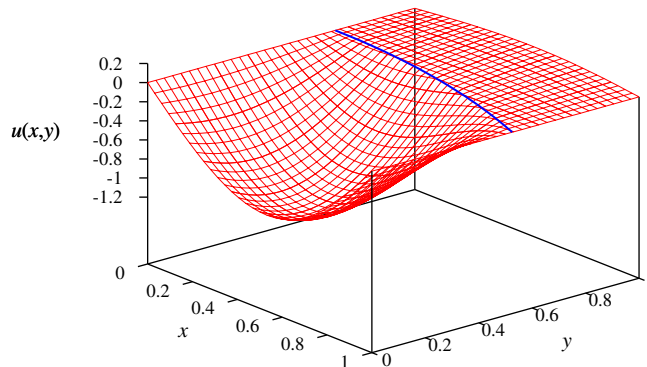


FIGURE 5 Exact solution (25) to the two-dimensional Poisson problem (24) with a discontinuity in the gradient along the line $y = \frac{\sqrt{2}}{2}(1 - \frac{1}{4}x^2)$.

If optimal rates of convergence are to be achieved then the curvature of the interface must be taken into account for the purposes of the integration, as discussed in section 2.2. Care must also be taken over the construction of the scheme's split subelements.

Just as in section 3.2, we use an isoparametric mapping from the discontinuity and the split sub-elements to the bulk element. For the integration scheme to be accurate we must place the vertices of these split sub-elements such that the discontinuity does not cross their interiors. Again, this scheme can be implemented in a straightforward fashion simply by summing over the knot points and weights. However, it is no longer always the case that the Jacobian of the coordinate transformations is constant in each element.

We reduce complexity by considering only elements that contain a single discontinuity. We also assume that when a discontinuity cuts an element it cuts precisely two of the element's edges. If either of these conditions are not met then typically the mesh may be locally refined until it is fine enough such that they are. We classify elements into three types:

1. those that are not cut by a discontinuity,
2. those that are cut by a discontinuity such that it crosses opposite element edges, and
3. those that are cut by a discontinuity such that it crosses adjacent element edges.

We assume that the discontinuity does not coincide with an element edge or vertex. This situation is unlikely to occur in most applications so it is a reasonable assumption to make. If it does, then perturbing by a small amount the value of the level set function at the vertices where the level set function is exactly zero will avoid such situations. Elements of type 1 need not be split. We split elements of type 2 into two rectangular subelements as shown in figure (a). We split elements of type 3 into two rectangular subelements and one triangular subelement, as in figure (b). If $B > A$ then we switch the coordinate directions to improve accuracy and maintain symmetry.

Integration over the triangular subelements was performed using tabulated knot points and weights of the appropriate order from⁵⁷, although others are readily available.

We use an explicit representation of Γ for the discontinuity for the purposes of integration. Inside a $(p + 1) \times (p + 1)$ -node rectangular element with basis functions of degree p we construct a $(p + 1)$ -node line element of order p that best describes the location of the discontinuity. Here the discontinuity lies along the line $y = y_c + vx^\alpha$, and with $\alpha = 2$ the position of the discontinuity is quadratic in the s -component of the bulk local coordinate. We can therefore exactly represent the location of the discontinuity for approximations of order $p \geq 2$. The choice of map that best approximates the location of discontinuities that are not exactly representable is more subtle and will be discussed later in section 6.1.

Note that the basis functions on Ω are polynomial in each of the local coordinate directions s, t . However, the Jacobian of the isoparametric mapping from the subelement to bulk element coordinate is not polynomial in s, t . It is well known that the exact integration property for Gauss-type quadrature of polynomials is lost for rectangular isoparametric elements^{53,54}. This means that the subelement quadrature is no longer exact, although it can still provide a good approximation if the mapping is carefully chosen^{53,54,58}. In particular, allowing the determinant of the Jacobian of the mapping to vary only in one coordinate direction is a sufficient requirement. For quadrilateral subelements this is equivalent to at least one pair of edges being parallel⁵³. The

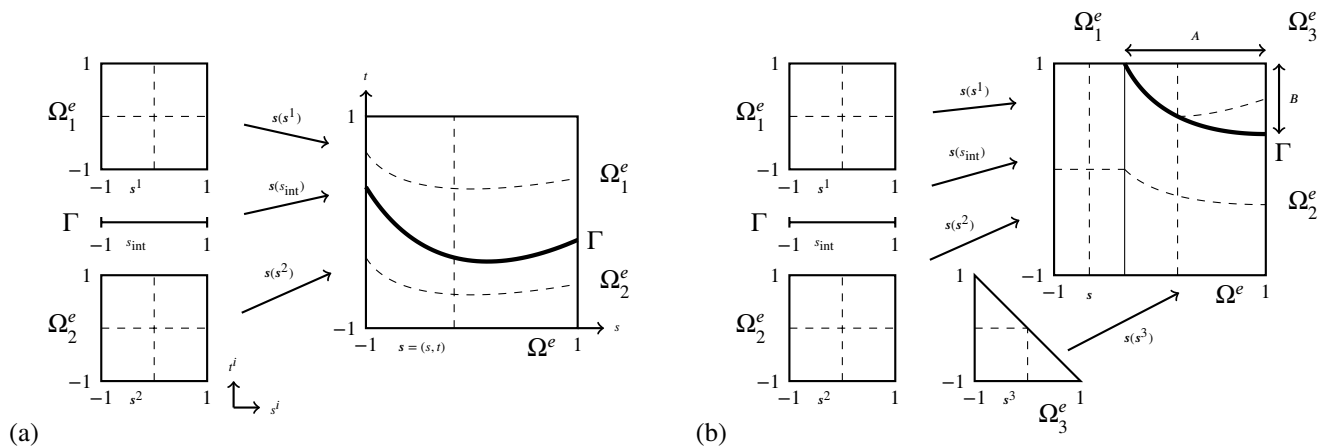


FIGURE 6 Elements Ω^e cut by a discontinuity Γ (right) and the mapping of the local coordinates on the explicit representation of the discontinuity and the split sub-elements Ω_i^e onto the bulk element (left). The dashed lines represent $s^i = 0$, $t^i = 0$.

decomposition shown in figure 6 satisfies this requirement by ensuring that each subelement has at most one curved side, and that all other sides align with a bulk local coordinate direction.

5.2 | Smoothness of the Approximation Space

The differences d_i in (20) are smooth. The correction polynomials are therefore continuous across element boundaries, and this ensures continuity of the improved modified enriched basis functions in the reproducing region (for conforming meshes). However, since the corrections are only applied in the reproducing region, care must be taken to ensure continuity at the boundary with the blending region.

Because the horizontal discontinuity in section 4 aligns with the element boundaries, the correction polynomials vanish at this boundary. The improved modified XFEM basis functions are therefore still continuous. But in general, the corrections do not vanish there. Instead we neglect contributions to the correction polynomials from the edge modes that correspond to these edges (i.e. those that are not cut by the discontinuity). These neglected contributions are ignored, and not subtracted from the modified XFEM basis functions. This regains continuity of the improved modified enriched basis functions at the boundary between the reproducing and blending regions.

Note that the set of modal basis functions used in the computation of the correction polynomials after spurious edge modes have been removed spans the space of polynomials of degree $2p$ that vanish along edges not cut by the discontinuity. We therefore expect that neglecting these spurious edge modes in the calculation of the correction polynomials will not adversely affect the rates of convergence that can be achieved using the improved modified basis functions, and this is demonstrated below.

5.3 | Error Analysis

The rates of convergence for the two-dimensional Poisson problem with a curved discontinuity, computed using our improved modified enriched basis functions and neglecting spurious edge modes, are shown in figure 7 and table 2. We have used values $y_c = \frac{\sqrt{2}}{2} + 0.005$, $v = \frac{\sqrt{2}}{8}$ and $\alpha = 2$. Notice that we have recovered optimal rates of convergence for approximations up to order $p = 4$, although the errors at the finest discretisations for $p = 4$ are greater than expected.

TABLE 2 Rates of convergence for the Poisson problem (6) in two dimensions with a curved discontinuity.²

p	1	2	3	4
L^2	2.00	2.99	3.99	4.91**
H^1 (Energy)	1.00	2.00	2.97	3.90**

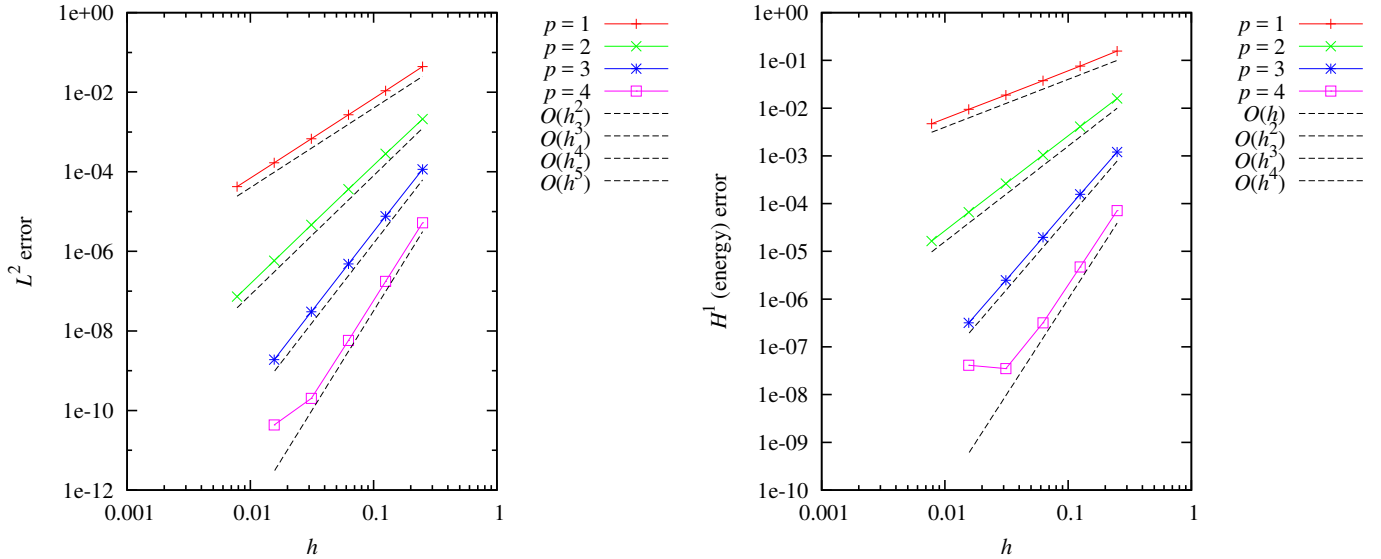


FIGURE 7 Rates of convergence in the L^2 (left) and energy (right) norms for the Poisson problem with a curved discontinuity using our improved modified XFEM basis functions for approximations up to order $p = 4$.

The reason for these elevated errors is that the XFEM is very sensitive to ill-conditioning under refinement, as noted in²⁵. Furthermore, the enriched basis functions can become almost linearly dependent when the discontinuity passes close to element edges or vertices. As a mesh is refined the elements become smaller and more numerous and the discontinuity is more likely to cross an element in an awkward fashion, passing very close to one of the nodes. This can dramatically affect the conditioning of the resulting system.

The same problem was solved with $y_c = \frac{\sqrt{2}}{2}$ and using quartic basis functions. In that case the Galerkin system matrix became suddenly very ill-conditioned, e.g. with condition number larger than 10^{18} , and so the solution was inaccurate. This resulted in a suboptimal rate of convergence. However, the effect of this inaccuracy was very localised. The majority of the global error in the solution was contributed by the patch of elements surrounding the troublesome node. Perturbing y_c by 0.005 avoids this situation, allowing the optimal rate of convergence to be seen over a larger range of mesh spacings h . In figure 7 we still see the effects of ill-conditioning in the solution at the finest mesh spacing at order $p = 4$, where the convergence rate becomes much lower than expected.

6 | A CIRCULAR WEAK DISCONTINUITY

Let us now consider a different physical problem. Let a circular elastic sheet be composed of two materials, as shown in figure 8. We solve the Navier-Lamé equations,

$$(\lambda + \mu)\nabla(\nabla \cdot \mathbf{u}) + \mu\nabla^2\mathbf{u} + \mathbf{F} = \mathbf{0}, \quad (26)$$

where λ and μ are the Lamé constants. We prescribe a uniform radial displacement $\mathbf{u} = \mathbf{x}$ on the outer boundary Γ_2 of the sheet, and calculate the displacement $\mathbf{u}(\mathbf{x})$ on the interior. We choose the physical constants in each material Ω_1, Ω_2 as follows: Young's modulus $E_1 = 1, E_2 = 10$ and Poisson's ratio $\nu_1 = 0.25, \nu_2 = 0.3$. From these physical parameters we can calculate the Lamé coefficients $\lambda_1 = \mu_1 = 0.4$, and $\lambda_2 = \frac{75}{13} \approx 3.8462, \mu_2 = \frac{50}{13} \approx 5.7692$. We also set the body force $\mathbf{F} = \mathbf{0}$. This problem is described in^{59,22,25}.

In order to calculate the exact solution, for prescribing the boundary conditions of the FE problem and for comparison with the FE solution, we move to a circular polar coordinate system. The Navier-Lamé equations then reduce to

$$\nabla(\nabla \cdot \mathbf{u}) = \mathbf{0},$$

²Rates of convergence are calculated from the last three points for each p as h decreases. Rates marked with ** are calculated after discarding the last two points.

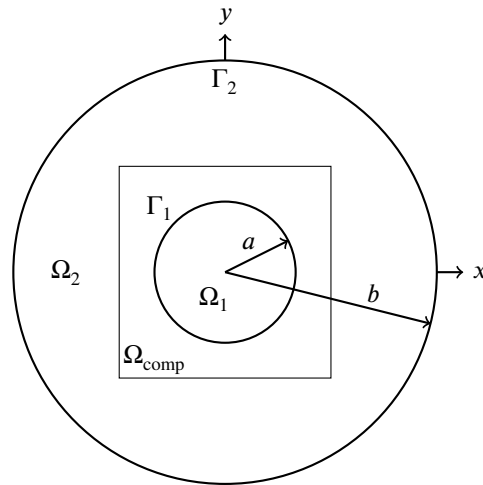


FIGURE 8 Bi-material boundary value problem. (Based on figure 7 from⁵⁹.)

or equivalently,

$$\frac{d}{dr} \left[\frac{1}{r} \frac{d}{dr} (ru_r) \right] = 0, \quad u_\theta = 0,$$

with prescribed displacement $u_r = r$ on the boundary Γ_2 . By considering displacement and traction continuity between the two materials the exact solution

$$u_r(r) = \begin{cases} \left[\left(1 - \frac{b^2}{a^2}\right) \gamma + \frac{b^2}{a^2} \right] r, & 0 \leq r \leq a, \\ \left[\left(1 - \frac{b^2}{r^2}\right) \gamma + \frac{b^2}{r^2} \right] r, & a \leq r \leq b, \end{cases} \quad (27a)$$

$$u_\theta = 0, \quad (27b)$$

where

$$\gamma = \frac{(\lambda_1 + \mu_1 + \mu_2)b^2}{(\lambda_2 + \mu_2)a^2 + (\lambda_1 + \mu_1)(b^2 - a^2) + \mu_2 b^2},$$

can be found, as described in⁵⁹. The horizontal and vertical components of this exact solution, after conversion back into the Cartesian coordinate system, are shown in figure 9

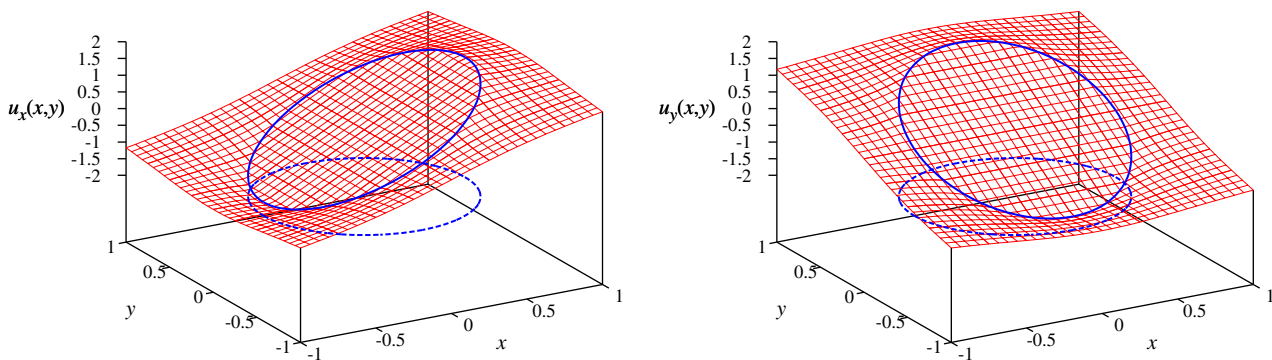


FIGURE 9 Horizontal (left) and vertical (right) components of the Cartesian form of the exact displacement solution (27a,b) to the linear elasticity problem (26) with a circular discontinuity.

6.1 | Explicit Representation of Curved Discontinuities

Recall that in section 5.1 we discussed how the split integration scheme used to evaluate functions with curved discontinuities requires the construction of an explicit representation that best describes the position of the discontinuity. Now that the discontinuity is not polynomially curved the interface representation can never be exact. Previously we used a mapping from the local coordinate s_{int} along the explicit representation to the bulk local coordinate $s = (s, t)$ that was linear in the s -direction. Doing the same for this circular interface leads to a poor approximation to the zero level set (figure 10(a)). Instead, we now use a mapping $s_{\text{int}} \mapsto \mathbf{s}$ that is linear in the arc-length coordinate along the discontinuity. The internal vertices of the explicit representation are placed at their ‘natural’ Gauss-Lobatto-Legendre⁵¹ (GLL) spacings along the discontinuity. This is shown in figure 10(b). For a circular discontinuity, the arc-length vertex spacing provides a much better approximation to its position. We expect that this alternative node positioning will provide the best approximation to arbitrarily curved discontinuities such as those that arise in two-phase flows or other physical problems.

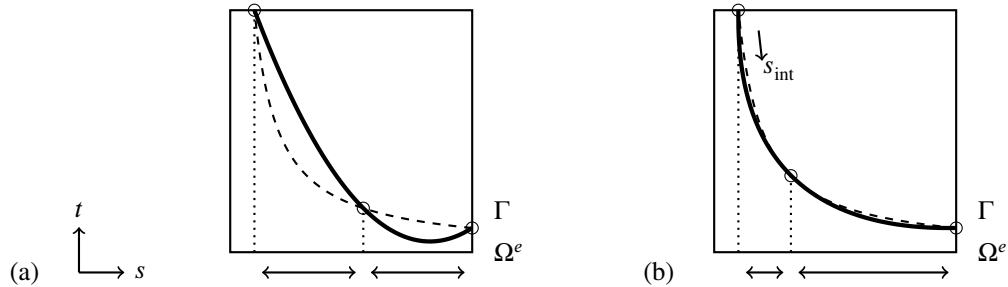


FIGURE 10 An explicit representation Γ of the position of a discontinuity located at the zero level of the level set function (shown as a curved dashed line). Circles mark the positions of the vertices of the explicit representation, placed at their ‘natural’ GLL-spacings $\{-1, 0, 1\}$ in the s -coordinate direction (left) and in the arc-length coordinate along the discontinuity (right).

This approach is very similar to that of Fries et al.⁴⁰ but rather than using linear or Hermite elements for the explicit representation of the interface, we use a line element of order p and GLL-spaced nodes. We also apply it in quadrilateral elements rather than triangular.

6.2 | Error Analysis

For the finite element approximation we solve the Cartesian Navier-Lamé equations (26) on a domain Ω_{comp} contained inside the outer disk (shown in figure 8) and prescribe the known exact displacements as boundary conditions. The energy norm we use for this linear elasticity problem is derived from the weak form of the Cartesian Navier-Lamé equations. We use the inner product

$$\langle u, v \rangle = \int_{\Omega} \mu \nabla u \cdot \nabla v \, d\Omega,$$

over our trial space $H^1(\Omega)$, and then define the energy norm³ $\|\cdot\|_E$ as

$$\|f\|_E = \langle f, f \rangle^{\frac{1}{2}} = \left[\int_{\Omega} \mu \nabla f \cdot \nabla f \, d\Omega \right]^{\frac{1}{2}}, \quad f \in H^1(\Omega),$$

where μ is one of the Lamé constants.

The rates of convergence in the L^2 and energy norms for the improved modified XFEM approximation applied to the two-dimensional linear elasticity problem are shown in figure 11 and table 3. We see that almost optimal rates of convergence are recovered. We attribute this slight suboptimality to the quality of the description of the discontinuity, and its effect on the integration, rather than to the construction of our improved modified XFEM enriched basis functions.

³This norm is again equivalent to the H^1 norm and to the other energy norm defined for the Poisson problem in section 3.1.

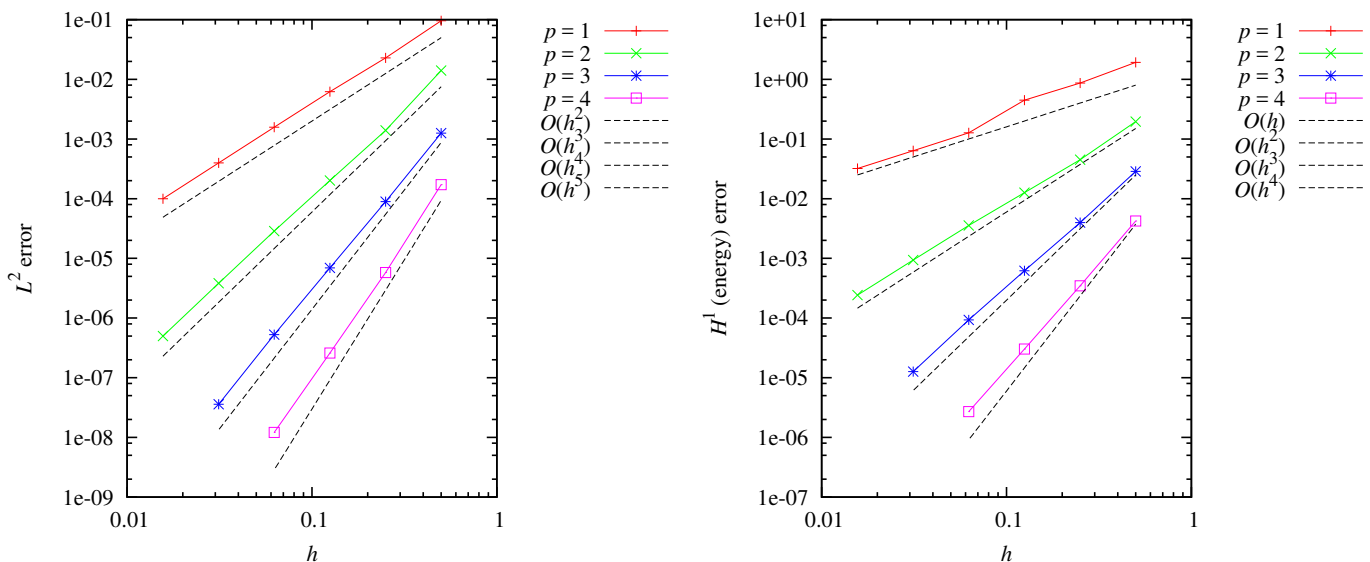


FIGURE 11 Rates of convergence in the L^2 (left) and energy (right) norms for the linear elasticity problem with a circular discontinuity using our improved modified XFEM basis functions for approximations up to order $p = 4$.

TABLE 3 Rates of convergence for the linear elasticity problem (26) with a circular discontinuity.

	p	1	2	3	4
L^2		1.99	2.92	3.79	4.45
H^1 (Energy)		0.99	1.94	2.81	3.50

7 | CONCLUSIONS

We set out to apply high-order finite element methods to discontinuous problems. The aim was to achieve the same optimal rates of convergence for problems involving arbitrarily aligned discontinuities as can be achieved for smooth problems. Immersed boundary methods were investigated as an alternative to boundary-fitted methods. Their use was motivated by the avoidance of remeshing for time-dependent problems. We then outlined how the XFEM with interface capturing via level sets enabled weak discontinuities to be included in approximations independently of the mesh. Several strategies for the resolution of the well-known problems in the blending region were discussed, and the modified XFEM was employed to resolve them. We then presented a method for improving the modified XFEM so that it was able to exactly represent piecewise polynomial functions of the same degree as the standard basis functions used in its construction. This was done by projecting out higher order contributions from the enrichment space so that spurious higher order contributions to the finite element approximation are avoided in the reproducing region. The coefficients of the resulting correction polynomials are independent of the equations that are being solved, and are expressed only in terms of the value of the level set function at element nodes. A numerical integration scheme that accurately integrates functions with curved discontinuities was also presented.

Together, the improved modified XFEM and the chosen discontinuous integration scheme allowed optimal rates of convergence to be recovered for Poisson problems with arbitrarily aligned straight and curved weak discontinuities for approximations of order $p \leq 4$. We then solved a linear elasticity problem with a circular weak discontinuity, achieving almost optimal rates of convergence for $p \leq 4$. These are the first truly optimally convergent results to be presented for a curved weak discontinuity, and also the first optimally convergent results of any kind that use the modified XFEM for approximations of order $p > 1$.

The improvements to the modified XFEM presented here are also applicable in three dimensions and we foresee the main challenge being the split integration of discontinuous functions over hexahedral elements. The number of ways that an interface can cut such elements in three dimensions is much larger, although recent work has tackled the problem of subcell quadrature in three dimensions^{43,39,44}.

We have demonstrated the potential for high-order XFEM approximations, and in particular the modified XFEM, to recover optimal rates of convergence for problems with straight and curved weak discontinuities. These high-order immersed methods are therefore a viable alternative to low-order approximations and boundary-fitted methods.

References

1. Wang ZJ, Fidkowski K, Abgrall R, et al. High-order CFD methods: current status and perspective. *Int J Numer Meth Fluid.* 2013;72:811–845.
2. Huynh HT, Wang ZJ, Vincent PE. High-order methods for computational fluid dynamics: A brief review of compact differential formulations on unstructured grids. *Comput Fluids.* 2014;98:209–220.
3. Karniadakis GEM, Sherwin S. *Spectral/hp Element Methods for Computational Fluid Dynamics*. Numerical Methods and Scientific Computation, Oxford University Press; second ed. 2005.
4. Saxby B. *hp-Adaptivity for Spectral Elements*. Master's thesis: School of Mathematics, The University of Manchester; 2010.
5. Belytschko T, Black T. Elastic crack growth in finite elements with minimal remeshing. *Int J Numer Meth Engng.* 1999;45:601–620.
6. Belytschko T, Chen H, Xu J, Zi G. Dynamic crack propagation based on loss of hyperbolicity and a new discontinuous enrichment. *Int J Numer Meth Engng.* 2003;58:1873–1905.
7. Chessa J, Wang H, Belytschko T. On the construction of blending elements for local partition of unity enriched finite elements. *Int J Numer Meth Engng.* 2003;57:1015–1038.
8. Laborde P, Pommier J, Renard Y, Salaün M. High-order extended finite element method for cracked domains. *Int J Numer Meth Engng.* 2005;64:354–381.
9. Osher S, Sethian JA. Fronts propagating with curvature-dependent speed: Algorithms based on Hamilton-Jacobi formulations. *J Comput Phys.* 1988;79:12–49.
10. Sethian JA. *Level Set Methods: Evolving Interfaces in Geometry, Fluid Mechanics, Computer Vision, and Materials Science*. Cambridge University Press; first ed. 1996.
11. Moës N, Dolbow J, Belytschko T. A finite element method for crack growth without remeshing. *Int J Numer Meth Engng.* 1999;46:131–150.
12. Claus S, Massing A, Burman E. CutFEM: a novel unfitted finite element formulation Presentation given at the 56th British Applied Mathematics Colloquium, 2014.
13. Becker R, Burman E, Hansbo P. A hierarchical NXFEM for fictitious domain simulations. *Int J Numer Meth Engng.* 2011;86:549–559.
14. Gracie R, Wang H, Belytschko T. Blending in the extended finite element method by discontinuous Galerkin and assumed strain methods. *Int J Numer Meth Engng.* 2008;74:1645–1669.
15. Babuška I, Caloz G, Osborn JE. *Special finite element methods for a class of second order elliptic problems with rough coefficients*. BN-1130: Institute for Physical Science and Technology, University of Maryland; 1992.
16. Babuška I, Caloz G, Osborn JE. Special finite element methods for a class of second order elliptic problems with rough coefficients. *SIAM J Numer Anal.* 1994;31:945–981.
17. Melenk JM, Babuška I. The partition of unity finite element method: basic theory and applications. *Comput Methods Appl Mech Eng.* 1996;139:289–384.
18. Babuška I, Melenk JM. The partition of unity method. *Int J Numer Meth Engng.* 1997;40:727–758.

19. Belytschko T, Moës N, Usui S, Parimi C. Arbitrary discontinuities in finite elements. *Int J Numer Meth Engng.* 2001;50:993–1013.
20. Saxby B. High-Order XFEM with Applications to Two-Phase Flows. PhD thesis: School of Mathematics, The University of Manchester; 2014.
21. Chahine E, Laborde P, Pommier J, Renard Y, Salaün M. Some Improvements of XFEM for Cracked Domains. In: :171–184Springer; 2007.
22. Legay A, Wang HW, Belytschko T. Strong and Weak arbitrary discontinuities in spectral finite elements. *Int J Numer Meth Engng.* 2005;64:991–1008.
23. Fries T-P. A Corrected XFEM approximation without problems in blending elements. *Int J Numer Meth Engng.* 2008;75:503–532.
24. Ventura G, Gracie R, Belytschko T. Fast integration and weight function blending in the extended finite element method. *Int J Numer Meth Engng.* 2009;77:1–29.
25. Cheng KW, Fries T-P. Higher-order XFEM for curved strong and weak discontinuities. *Int J Numer Meth Engng.* 2010;82:564–590.
26. Moës N, Cloirec M, Cartraud P, Remacle JF. A computational approach to handle complex microstructure geometries. *Comput Methods Appl Mech Eng.* 2003;192:3163–3177.
27. Tarancón JE, Vercher A, Giner E, Fuenmayor FJ. Enhanced blending elements for XFEM applied to linear elastic fracture mechanics. *Int J Numer Meth Engng.* 2009;77:126–148.
28. Fries T-P, Belytschko T. The generalized/extended finite element method: An overview of the method and its applications. *Int J Numer Meth Engng.* 2010;84:253–304.
29. Vejchodská T, Šolín P. Static condensation, partial orthogonalization of basis functions, and ILU preconditioning in the *hp*-FEM. *J Comput Appl Math.* 2008;218:192–200.
30. Chahine E, Laborde P, Renard Y. A non-conformal eXtended Finite Element approach: Integral matching Xfem. *Appl Numer Math.* 2011;61:322–343.
31. Hansbo A, Hansbo P. An unfitted finite element method, based on Nitsche’s method, for elliptic interface problems. *Comput Methods Appl Mech Eng.* 2002;191:5537–5552.
32. Nitsche J. Über ein Variationsprinzip zur Lösung von Dirichlet-Problemen bei Verwendung von Teilräumen, die keinen Randbedingungen unterworfen sind. *Abh Math Sem Univ Hamburg.* 1971;36:9–15.
33. Babuška I, Banerjee U, Kergrene K. Strongly stable generalized finite element method: Application to interface problems. *Comput Methods Appl Mech Eng.* 2017;327:58–92.
34. Lehrenfeld C, Reusken A. Analysis of a high-order unfitted finite element method for elliptic interface problems. *IMA J Numer Anal.* 2017;00:1–37.
35. Dolbow J, Moës N, Belytschko T. An extended finite element method for modeling crack growth with frictional contact. *Comput Methods Appl Mech Eng.* 2001;190:6825–6846.
36. Stazi FL, Budyn É, Chessa J, Belytschko T. An extended finite element method with higher-order elements for curved cracks. *Comput Mech.* 2003;31:38–48.
37. Zi G, Belytschko T. New crack-tip elements for XFEM and applications to cohesive cracks. *Int J Numer Meth Engng.* 2003;57:2221–2240.
38. Jiang W, Annavarapu C, Dolbow JE, Harari I. A robust Nitsche’s formulation for interface problems with spline-based finite elements. *Int J Numer Meth Engng.* 2015;104:676–696.

39. Fries T-P, Omerović S. Higher-order accurate integration of implicit geometries. *Int J Numer Meth Engng.* 2016;106:323–371.
40. Fries T-P, Omerović S, Schöllhammer D, Steidl J. Higher-order meshing of implicit geometries–Part I: Integration and interpolation in cut elements. *Comput Methods Appl Mech Eng.* 2017;313:759–784.
41. Fries T-P. Higher-order conformal decomposition FEM (CDFEM). *Comput Methods Appl Mech Eng.* 2018;328:75–98.
42. Soghrati S, Duarte CA, Geubelle PH. An adaptive interface-enriched generalized FEM for the treatment of problems with curved interfaces. *Int J Numer Meth Engng.* 2015;102:1352–1370.
43. Kudela L, Zander N, Kollmannsberger S, Rank E. Smart octrees: Accurately integrating discontinuous functions in 3D. *Comput Methods Appl Mech Eng.* 2016;306:406–426.
44. Paul B, Ndeffo M, Massin P, Moës N. An integration technique for 3D curved cracks and branched discontinuities within the extended Finite Element Method. *Finite Elem Anal Des.* 2017;123:19–50.
45. Ndeffo M, Massin P, Moës N, Martin A, Gopalakrishnan S. On the construction of approximation space to model discontinuities and cracks with linear and quadratic extended finite elements. *Adv Model Simul Eng Sci.* 2017;4:6.
46. Byfut A, Shröder A. *hp*-adaptive extended finite element method. *Int J Numer Meth Engng.* 2012;89:1392–1418.
47. Dréau K, Chevaugeon N, Moës N. High order extended finite element method: influence of the geometrical representation. In: ; 2008; Venice, Italy.
48. Chopp DL. Computing Minimal Surfaces via Level Set Curvature Flow. *J Comput Phys.* 1993;106:77–91.
49. Sussman M, Smereka P, Osher S. A level set approach for computing solutions to incompressible two-phase flows. *J Comput Phys.* 1994;114:146–159.
50. Babuška I, Suri M. The *p*- and *h-p* versions of the Finite Element Method, basic principles and properties. *SIAM Rev.* 1994;36(4):578–632.
51. Abramowitz M, Stegun IA. *Handbook of Mathematical Functions with Formulas, Graphs, and Mathematical Tables.* Chichester: Wiley; 1972.
52. Sukumar N, Moës N, Moran B, Belytschko T. Extended finite element method for three-dimensional crack modelling. *Int J Numer Meth Engng.* 2000;48:1546–1570.
53. Ventura G. On the elimination of quadrature subcells for discontinuous functions in the eXtended Finite-Element Method. *Int J Numer Meth Engng.* 2006;66:761–795.
54. Bathe K-J. *Finite Element Procedures.* Prentice Hall; 1996.
55. Ducker L. Level sets and the finite element method. Master's thesis: School of Mathematics, The University of Manchester; 2006.
56. Wolfram Research, Inc. *Mathematica* Version 9.0, Champaign, Illinois, 2012.
57. Dunavant DA. High degree efficient symmetrical Gaussian quadrature rules for the triangle. *Int J Numer Meth Engng.* 1985;21:1129–1148.
58. Ciarlet PG. *The Finite Element Method for Elliptic Problems.* SIAM; 2002.
59. Sukumar N, Chopp DL, Moës N, Belytschko T. Modeling holes and inclusions by level sets in the extended finite-element method. *Comput Methods Appl Mech Eng.* 2001;190:6183–6200.

How to cite this article: Saxby BA., and Hazel AL. (2018), Improving the Modified XFEM for Optimal High-Order Approximation, *Int J Numer Meth Engng.*, 2018;00:1–23.